JOURNAL OF SOLID STATE CHEMISTRY 53, 76–86 (1984)

An Electron-Optical Study of Nickel Monosulfide

S. N. BLACK AND D. A. JEFFERSON

Department of Physical Chemistry, Lensfield Road, Cambridge CB2 1EP

AND P. HENDERSON

Department of Mineralogy, British Museum (Natural History) Cromwell Road, London SW7 5BD, United Kingdom

Received August 17, 1983; in revised form January 9, 1984

The high temperature form of nickel monosulfide, $Ni_{(1-x)}S$ has the nickel arsenide structure. It is nonstoichiometric in the range NiS–$Ni_{0.91}S$. Powder X-ray diffraction of synthetic samples suggests a simple solid solution, but high resolution electron microscopy reveals three different structural regions. One of these, previously reported elsewhere, has rhombohedral symmetry with a $3 \times a$ repeat. The second region shows a $2 \times a$ repeat, while the third appears to contain disordered vacancies. The effect of multiple scattering on the electron diffraction patterns and images is discussed.

Introduction

α-NiS is the high-temperature form of nickel monosulfide. It has the nickel arsenide structure (Fig. 1), based on the close-packing of sulfur atoms. The sulfurs lie in hexagonally close-packed layers, which are stacked in the "*ABABA . . .*" fashion to give a hexagonal unit cell. The nickel atoms occupy the octahedral interstices, of which there are two per unit cell, lying on planes perpendicular to the z-axis, exactly halfway in between the planes of sulfur atoms. The structure has space group $P6_3/mmc$ with a sixfold screw axis and perpendicular glide planes, giving rise to the systematic absence condition $h + k = 3n$, $1 =$ odd (*1*).

The Ni–S phase diagram was determined accurately by Kullerud (Fig. 2) (*2*) and has been confirmed more recently (*3*). α-NiS shows nonstoichiometry in the range NiS–$Ni_{0.91}S$, the unit cell size decreasing with decreasing nickel content, consistent with the formation of cation vacancies. Hence the phase is often referred to as $Ni_{(1-x)}S$, as it will be hereafter. Cation deficiency in the nickel arsenide structure is common, as the structure can readily accommodate vacant octahedral sites and many compounds with this basic structure exhibit superstructures arising from ordering of the vacancies (*4*); for example, the chromium sulfides (*5*) and the iron sulfides (*6*). Ordering of the vacancies into alternate layers of cations causes the systematic absence condition to be broken and the (001) spot appears weakly.

$Ni_{(1-x)}S$ was discovered in 1923 (*7*). It does not occur in nature, it transforms to the mineral millerite upon slow cooling (*8*). It is readily quenchable and stable for many months at room temperature. The properties of $Ni_{(1-x)}S$ are strongly dependent on composition. As seen from the phase diagram (Fig. 2) the temperature of the transi-

0022-4596/84 $3.00

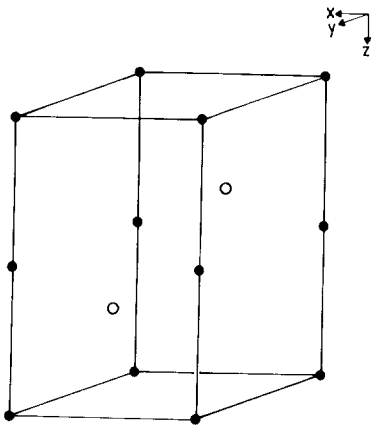

FIG. 1. The nickel arsenide structure. Filled circles represent nickel atoms, open circles represent sulfur atoms.

tion to millerite varies markedly with composition. Quenched samples of the stoichiometric compound show a metal to semi-metal transition at −10°C; this transition temperature decreases to −269°C with decreasing nickel content (*9*). There are inconsistencies in the literature concerning the physical properties associated with this transition (*10, 11*).

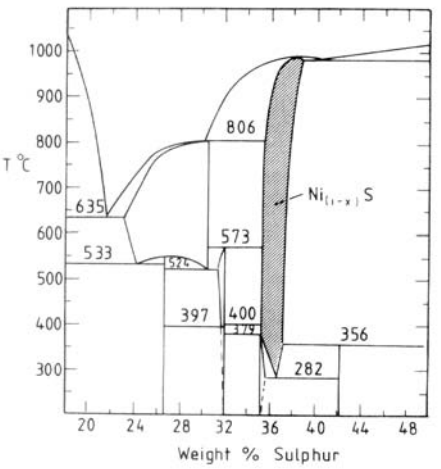

FIG. 2. The central portion of the nickel–sulfur phase diagram, after Kullerud (*2*). Stoichiometric α-NiS and millerite contain 35.3 weight% sulfur.

Whereas for $Fe_{(1-x)}S$ the unit cell dimensions may be used to give a reliable composition (*12*); Kullerud (*2*) found that this was not possible for $Ni_{(1-x)}S$. This was owing to a phase transformation within the $Ni_{(1-x)}S$ region of the phase diagram at about 750°C, which could not, however, be detected by differential thermal analysis (*2*). A $3a3a3c$ superstructure of $Ni_{(1-x)}S$ was detected subsequently by X-ray diffraction (*13*). Samples prepared in a controlled sulfur at-

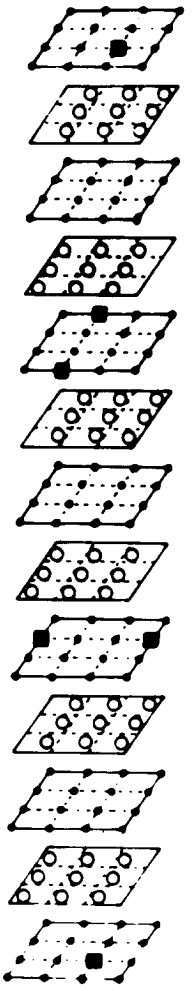

FIG. 3. The $3a3a3c$ structure. Filled circles represent nickel atoms, open circles represent sulfur atoms. Filled squares represent vacant nickel sites. The structure has stoichiometry $Ni_{17}S_{18}$ and space group $R32$.

mosphere have been examined by X-ray diffraction and electron diffraction by Noda *et al.* (*14*). Collin *et al.* (*15*) have also studied the phase by X-ray diffraction. Each group found an ordered $3a3a3c$ region and a disordered region and independently proposed the same structure model for the $3a3a3c$ supercell, based on the stoichiometry $Ni_{17}S_{18}$ and with space groups $P3_121$ and $P3_221$ (Fig. 3). It was suggested that the more-ordered phase was more stable at higher temperatures, and that both phases showed variable stoichiometry (*14*). The structure model has been refined recently by X-ray diffraction of a twinned crystal, and an analysis of the observed stacking faults has been proposed (*16*).

The aim of this work was to discover the structural modifications which enable $Ni_{(1-x)}S$ to accommodate nonstoichiometry. X-Ray diffraction alone proved inadequate so additional compositional and structural information was sought. No high resolution electron microscopy had previously been reported on this phase; due perhaps in part to the observation that some nickel sulfides are unstable in the electron beam (*17*). However, in view of the success of electron microscopy in the study of the iron sulfides (*6*), an investigation was undertaken using primarily this technique.

Results

The samples were prepared by direct synthesis of the elements, which were obtained at 99.5% purity. They were mixed in the appropriate proportions, and ground together. From 2 to 3 g of the mixture was placed in a cylindrical silica tube; this was sufficient to fill two-thirds of the tube. The tubes were evacuated, sealed, and placed in a steel tube inside a horizontal furnace. The temperature was controlled by a thermocouple placed inside the steel tube, and was maintained at 750°C for the preparations. Samples were quenched by dropping the silica tubes into cold water. No traces of condensed sulfur were observed on the tube walls.

Samples were analyzed initially by powder X-ray diffraction in a Philips APD-10 diffractometer. All peaks could be indexed on the nickel arsenide unit cell. The unit cell parameters, a and c, were consistent with those reported by Kullerud (*2*).

The compositions of the samples were obtained by electron microprobe analysis. Grain mounts of the samples were polished and analyzed in a Cambridge Instruments Mark 9 wavelength dispersive probe. Pyrite and nickel metal standards were used. The electron microprobe and X-ray powder data are summarized in Table I.

The synthesized samples appeared homogeneous within the limits of detection of these techniques. The microprobe analyzed regions of about 5 μm diameter; the consistency of the microprobe data suggests a single phase. The microprobe gave absolute compositions and showed no evidence of any impurities.

Samples were examined by electron diffraction, energy dispersive analysis (EDA), and high resolution imaging in a JEOL 200-CX electron microscope fitted with a high resolution side-entry goniometer which has sufficient tilt to enable the [100] and [1$\bar{1}$0] zone axis patterns from the same crystal to be recorded. Figure 4 shows electron diffraction patterns down [100], [1$\bar{1}$0], and [001]. Together these patterns allow unequivocal construction of the reciprocal lat-

TABLE I

UNIT CELL DIMENSIONS AND COMPOSITIONS

Nominal composition	$Ni_{0.95}S$[a]	NiS
Composition by microprobe	$Ni_{0.93(1)}S$[b]	$Ni_{0.99(1)}S$
Unit cell size, a:	3.429(2)	3.448(2)
Unit cell size, c:	5.325(7)	5.359(3)

[a] Results for $Ni_{0.95}S$ are the average for three samples.

[b] Standard deviations are given in parentheses.

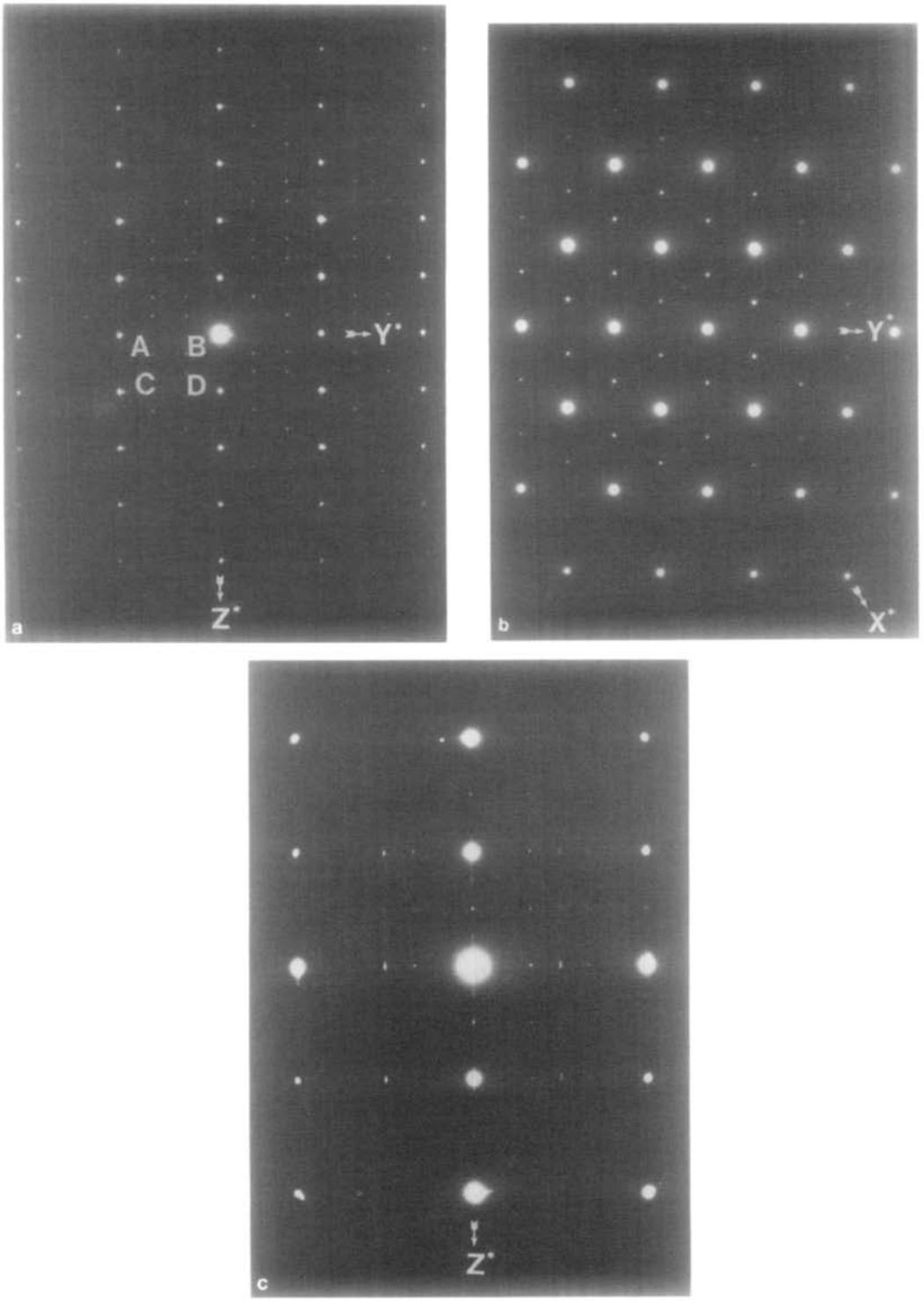

FIG. 4. Electron diffraction patterns of $Ni_{(1-x)}S$, taken down three different zone axes: (a) [100], (b) [001], (c) [1$\bar{1}$0].

tice, which in addition to the expected nickel arsenide pattern shows three interesting features:

(a) Spots A–D indicate the presence of a $3a3a3c$ superlattice.

(b) There are streaks parallel to z^* along $(0,0,l)$ rows, and also along $(1/2, 0, l)$ rows.

(c) The (001) spots are strong.

These results are discussed in more detail below. However, it seemed unlikely that the streaks and the superlattice spots originated from the same region, unless an extremely complex structure was present, so lattice images were obtained. Figure 5 shows one such image displaying three structural regions; an optical diffraction pattern is shown for each.

(i) The $3a3a3c$ region. This region shows (001) and inclined fringes, and the optical diffraction pattern indicates a $3a3a3c$ superlattice with rhombohedral symmetry.

(ii) The $2a2anc$ region. The streaks arise solely from this region which resembles a defect. The white dots in the image are separated by $2a$; this is consistent with the appearance of extra streaks along the $(0, 1/2, l)$ row.

(iii) The disordered region. This region shows neither superlattice nor defects. It has the simple nickel arsenide lattice. The (001) spot is strongly present in the optical diffraction pattern, and the (001) fringes dominate the image.

An attempt was made to obtain compositional information from these three regions using EDA. The detector was first calibrated using a stoichiometric sample. The variation in analysis from crystal to crystal was ±5% for these elements. The compositional differences to be expected in this sample are small, in the range $Ni_{0.91}S$–NiS. The three regions were finely intergrown, individual regions never being larger than 1000 Å across. Hence it was not surprising that this technique failed to give any meaningful compositional information.

The presence of three structural regions precludes the possibility that this is an equilibrium assemblage. Therefore, further samples were prepared and studied in order to provide more information about the structures and relative stabilities of these regions.

Discussion

The 3a3a3c Region

The optical diffraction pattern shown here (Fig. 5) has rhombohedral symmetry. Collin (*16*) reported that spots at (0, 1/3, 0), etc. were weakly present, but they were not observed here. This suggests that, for the material studied here, the space group $R32$ is more likely than that previously proposed (*14, 15*). This is also the correct space group for the idealized model (Fig. 3). Patterns such as those in Fig. 4 are obtained if both obverse and reverse orientations of the superlattice are present. Simple twinning of the two orientations was not observed in the images; they were always separated by slabs of the $2a2anc$ structure.

A sample containing the $3a3a3c$ regions was annealed at 750°C to try and obtain an equilibrium assemblage. Electron diffraction studies showed that after annealing, only the $2a2anc$ and disordered regions remained; the ordered superlattice had apparently transformed. To investigate the possibility that the $3a3a3c$ structure was more stable at higher temperatures, as reported by Noda *et al.* (*14*), two samples were annealed at 900°C. They showed two different results; in one the $3a3a3c$ superlattice appeared, in the other a weaker, incommensurate superlattice was observed (Fig. 6), which closely resembles the $3a3a3c$ superlattice. It shows the $3c$ repeat, but is incommensurate in a. Following the nomenclature of Morimoto (*6*), it may be described as a $2.6a$ lattice. In order to accommodate variable stoichiometry and preserve the $3c$ repeat, such incommensurate behavior is necessary.

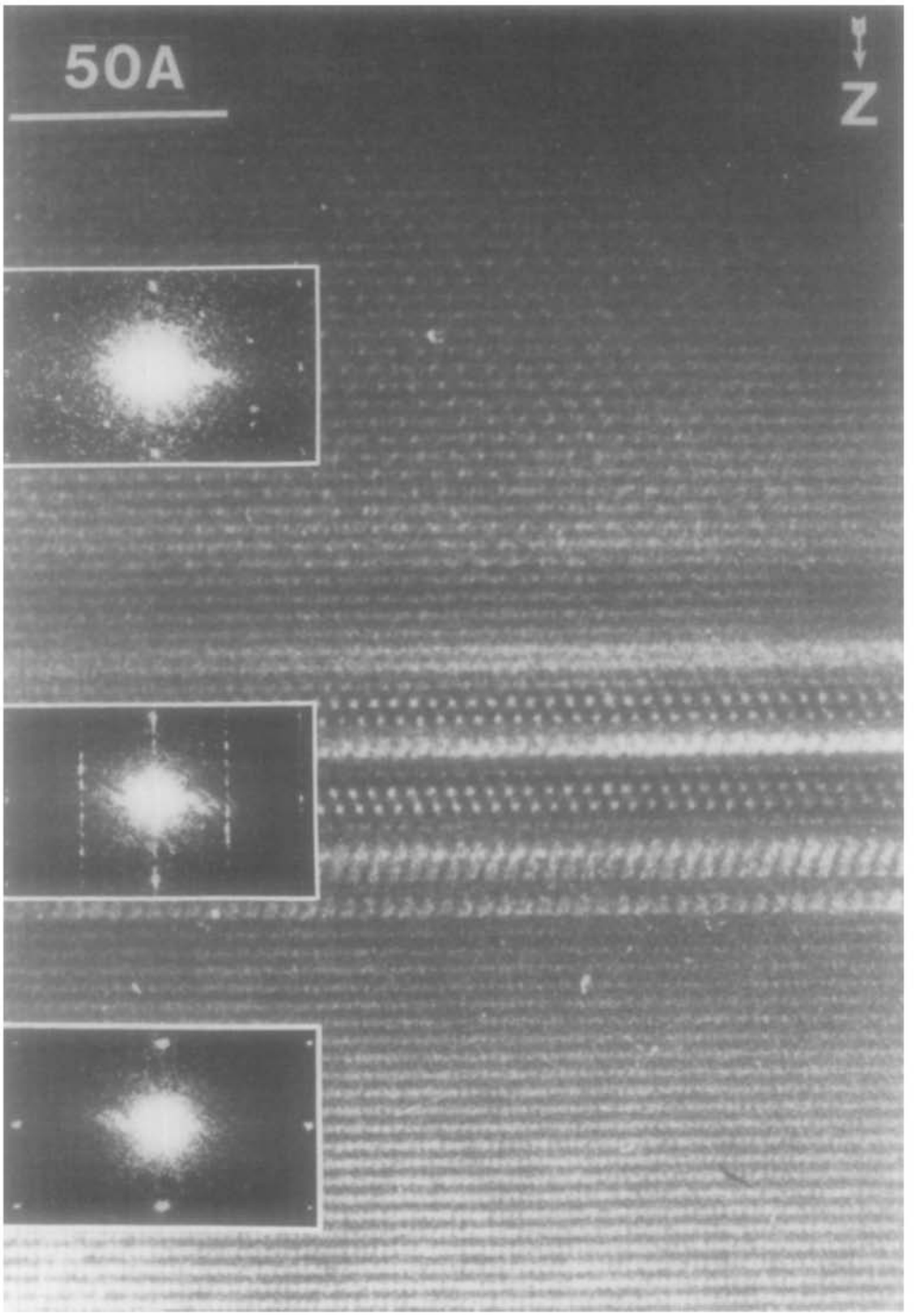

FIG. 5. Lattice image of $Ni_{(1-x)}S$, taken down [100], showing three different regions. The $3a3a3c$ region is uppermost, the $2a2anc$ region is in the middle and the disordered region is at the bottom. An optical diffraction pattern is shown for each region.

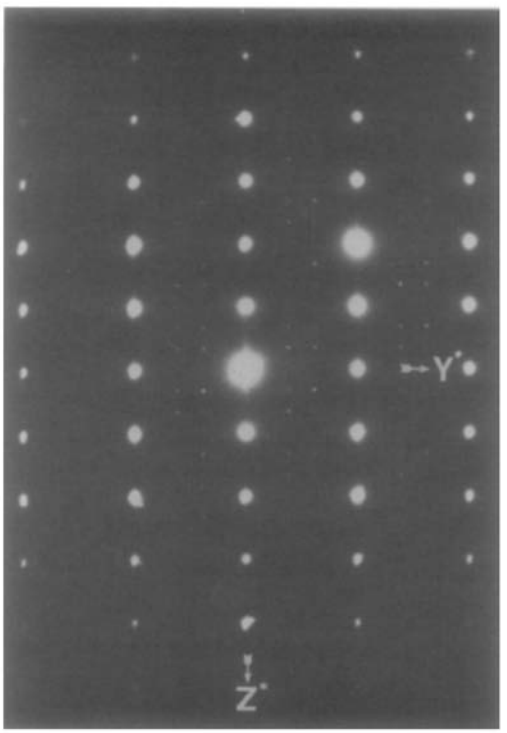

FIG. 6. Electron diffraction pattern taken down [100], showing the $3c$ repeat and an incommensurate a repeat.

The 2a2anc Region

Noda (*14*) and Collin (*15*) both observed streaks along (0, 0, *l*) and also along (*0, 1/2, l*) rows, indicating a $2a2anc$ structure. A $2a2a3c$ superstructure has been reported for iron sulfide (Fig. 7) (*18*), which requires the stoichiometry Fe_7S_8. The corresponding stoichiometry Ni_7S_8 lies outside the composition range of $Ni_{(1-x)}S$. An attempt to prepare it produced, as found by other workers (*2*), a mixture of $Ni_{(1-x)}S$ and NiS_2.

Optical diffraction on the lattice image (Fig. 5) shows that the streaks come from the narrow slabs of crystal which show the $2a$ repeat. The streaks indicate random stacking along the z axis. Further micrographs, of which Fig. 8 is typical, enable these regions to be characterized as follows:

(i) They are always perpendicular to the z axis.

(ii) They have variable width along z. Some are up to 70 Å wide, though more usually they are 15–20 Å.

(iii) They are randomly distributed within the crystals.

(iv) They all show unusual strong contrast which varies across their width.

Samples of nominally stoichiometric NiS did not contain these regions. Consequently ordering of vacancies must be responsible for the $2a$ repeat. This repeat suggests a large number of vacancies and it seems likely that the regions are composed of a highly disordered structure derived from the $2a2a3c$ structure, in which the vacancies are separated by $2a$ within the layers, but the layers are stacked randomly. This proposal is tentative, as it cannot be supported by direct compositional evidence, or by computer simulation of images (see below).

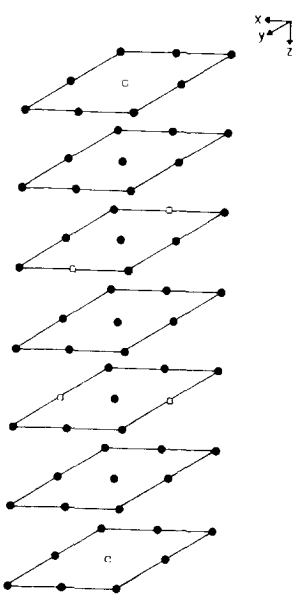

FIG. 7. The $2a2a3c$ structure. Sulfur atoms are omitted for clarity. Filled circles represent nickel atoms, open squares represent vacant nickel sites. The structure has stoichiometry Ni_7S_8.

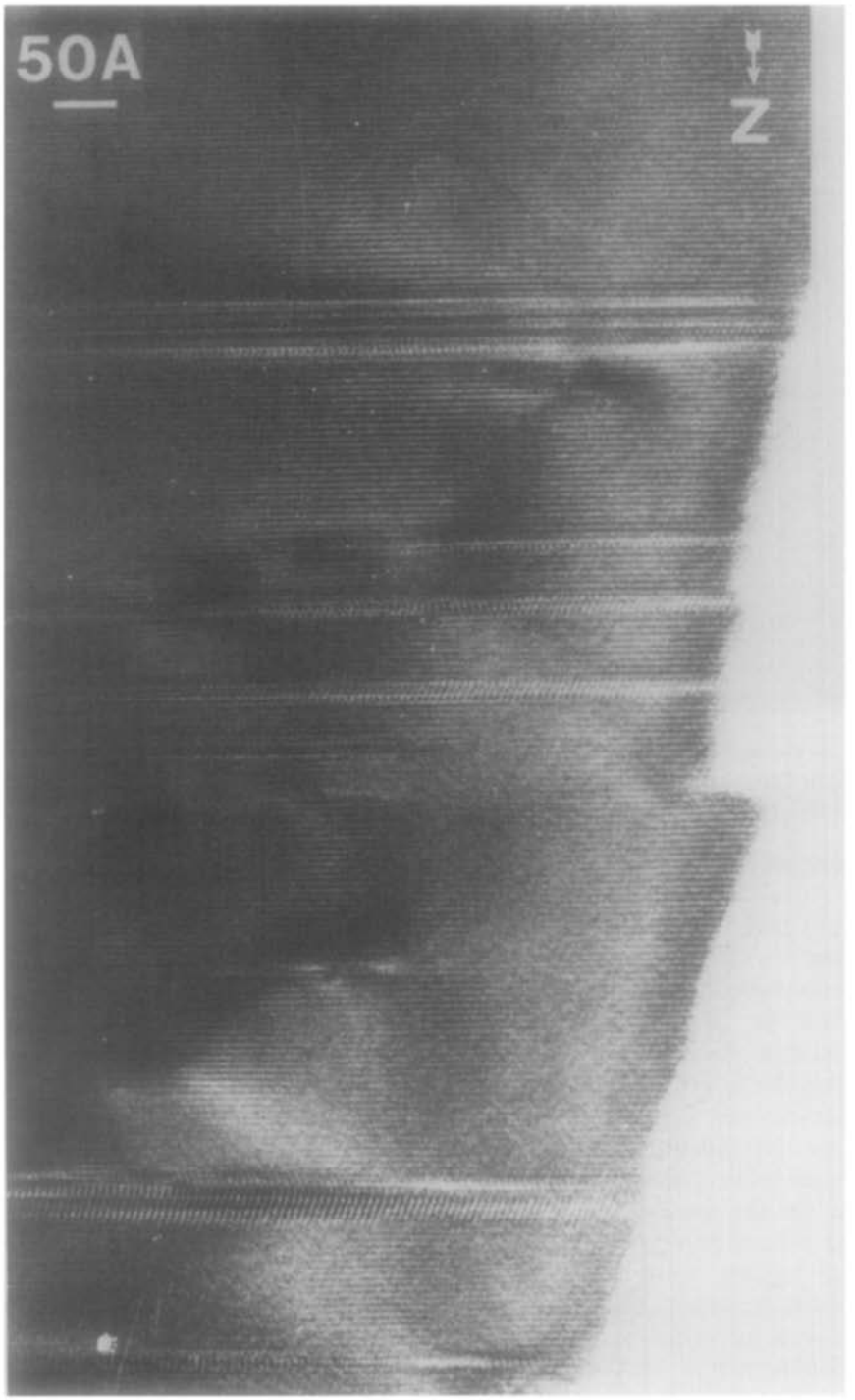

FIG. 8. Lattice image of an annealed sample of $Ni_{(1-x)}S$. Slabs of the $2a2anc$ structure, with various widths, are intergrown randomly with the disordered regions.

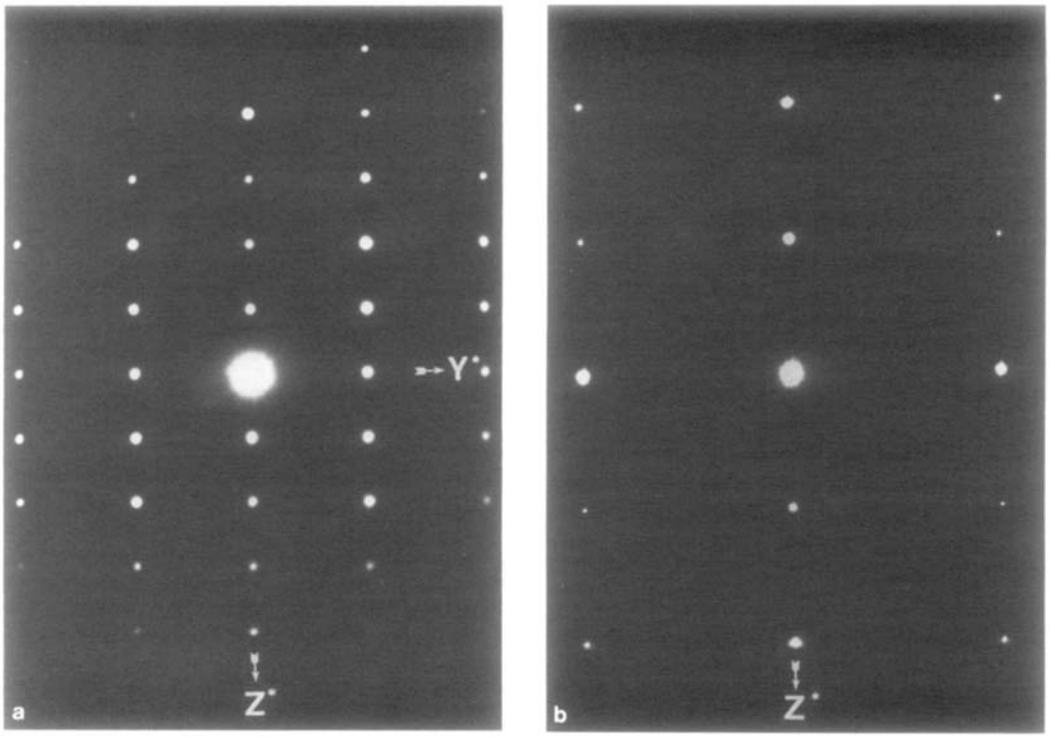

FIG. 9. Electron diffraction patterns of NiS, taken from the same crystal down two different zone axes: (a) [100], (b) [1$\bar{1}$0]. There are neither streaks nor superlattice spots. The (001) spot is present down [100], but absent down [1$\bar{1}$0].

The Disordered Region

There are three possible structures for this region: (i) stoichiometric NiS, (ii) $Ni_{(1-x)}S$ with completely disordered vacancies, and (iii) $Ni_{(1-x)}S$ with vacancies which are ordered into alternate layers but disordered within the layers.

Structures (i) and (ii) cannot be distinguished by crystallographic techniques, other than accurate absolute intensity measurements. In the annealed samples, the disordered regions predominate, and if the disordered regions were stoichiometric, then annealed samples would contain more $2a2anc$ regions in order to preserve the overall stoichiometry. This was not observed; hence compositional evidence favors (ii).

It was hoped that electron diffraction would be able to distinguish between structures (ii) and (iii). For structure (ii), the (001) spot should be absent, for structure (iii) it should be present but weak. To check this, a sample of nominally stoichiometric NiS was examined by electron diffraction. Figure 9 shows zone axis patterns down [100] and [1$\bar{1}$0] taken from the same crystal. They show that the (001) spot is strong in [100] and absent in [1$\bar{1}$0]. The presence of the (001) spot in [100] must be due to multiple scattering. Therefore the [100] zone cannot be used to distinguish between the two structures.

An annealed sample was subsequently examined; large disordered regions were sought which could be titled to [1$\bar{1}$0]. The diffraction patterns obtained were identical to that shown in Fig. 9b. The (001) spot was absent, favoring structure (ii).

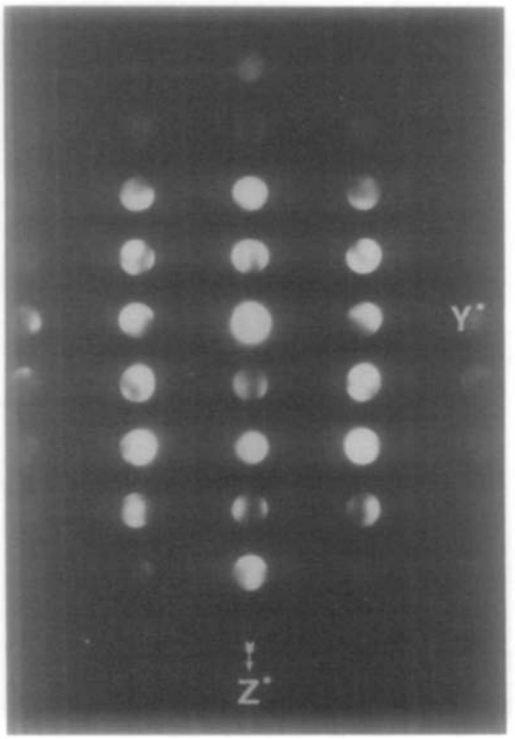

FIG. 10. Defocussed diffraction pattern from a disordered region, taken down [100]. There is a dark line parallel to z^* through the (001) spot.

An attempt was made to simulate the images using the multislice technique (*19*). It was not possible to match images taken down [100]. It was noted that the computed diffraction pattern for structure (ii) still showed (001) as absent, even allowing for dynamical scattering, this being a similar problem to that of rutile (*20*). The extinction condition is due to a glide plane; hence the (001) spot is kinematically and dynamically forbidden (*21*). Its presence must be due to a loss of symmetry caused by beam tilt, crystal tilt, crystal bending, or crystal shape. In unusually flat crystals it was possible to observe a dark band running through the center of the (001) spot (Fig. 10). This "Gjonnes–Moodie line" indicates that the glide plane is still present, again favoring structure (ii).

Unfortunately, the (001) fringes are the dominant feature of all the images obtained (Figs. 5 and 8). The intensity of these fringes cannot be simulated by simple multislice calculations. More complicated multislice calculations to allow for possible asymmetries include too many variables to be meaningful. This problem affects images of all three regions taken down [100]. As the unit cell is so small, imaging down other axes (e.g., $[1\bar{1}0]$) can only give fringes in one direction with the resolution available at 200 kV.

Conclusions

Three different structures were observed in nickel monosulfide, $N_{(1-x)}S$. The $3a3a3c$ structure observed here was found to have rhombohedral symmetry corresponding to space group $R32$. The model previously proposed (*14*, *15*) also has this symmetry. Related structures were observed which preserve the $3c$ repeat but have an incommensurate a repeat. This may correspond to variable stoichiometry.

The $2a2anc$ structure has been characterized. It only exists in narrow slabs lying perpendicular to z. Indirect compositional evidence suggests that this structure has a high vacancy concentration. This is consistent with the observed $2a$ repeat which is due to vacancy ordering. The exact structure of these regions is still unclear, and further studies, especially those involving higher accelerating voltages to achieve ca. 2.0 Å resolution are continuing.

The available electron diffraction evidence suggests that the disordered structure does not contain any ordered vacancies. Indirect compositional evidence suggests that the disordered regions are nonstoichiometric. Therefore it seems likely that these regions contain completely disordered vacancies, though it is impossible to confirm this unequivocally.

The $3a3a3c$ superstructure appears to

form initially at temperatures higher than 750°C, possibly with some incommensurability in the (001) planes owing to compositional variations. The two possible orientations of the $3a3a3c$ structure are invariably separated by slabs of the $2a2anc$ structure. At lower temperatures these slabs persist, but the $3a3a3c$ structure transforms to the disordered structure.

This is the reverse of the case in iron sulfides, where the disordered high temperature phase gives rise to ordered superstructures at lower temperatures (*6*). In $Ni_{(1-x)}S$ some other effect much outweigh configurational entropy considerations.

Electron diffraction and lattice imaging have revealed considerable structural complexity in $Ni_{(1-x)}S$, which must be considered in studies of its physical properties. In particular the temperature of preparation will determine whether or not the quenched product will contain the $3a3a3c$ superlattice. Brusetti (*11*), using a final annealing temperature of 600°C, reported specific heat values for quenched samples which were consistent with those of Ohtani (*10*) whose samples were prepared by heating at 723°C for 1 week. It is possible that this discrepancy is related to the different structures present in $Ni_{(1-x)}S$.

Acknowledgments

The authors thank Professor J. M. Thomas for his encouragement with this work, and for making available the facilities in the Department of Physical Chemistry. The comments of Dr. M. K. Uppal, Dr. O. Terasaki, and Dr. W. M. Stobbs were very helpful and much appreciated. One of us (SNB) acknowledges the financial support of the S.E.R.C.

References

1. "International Tables for X-Ray Crystallography," Vol. I, 3rd ed. p. 304. Kynock Press, Birmingham (1976).
2. G. KULLERUD AND R. A. YUND, *J. Petrol.* **3,** 126 (1962).
3. R. Y. LIN, D. C. HU, AND Y. A. CHANG, *Metall. Trans. B* **9B**(4), 531 (1978).
4. A. F. WELLS, "Structural Inorganic Chemistry," 4th ed., 609. Oxford Univ. Press (Clarendon), Oxford (1975).
5. F. JELLINEK, *Acta Crystallogr.* **10,** 620 (1957).
6. N. MORIMOTO, *Mem. Inst. Sci. Ind. Res. Osaka Univ.* **35,** 45 (1978).
7. N. ALSEN, *Geol. Foeren. Stockholm Forh.* **45,** 606 (1923).
8. W. BLITZ, *Z. Anorg. Chem.* **228,** 275 (1936).
9. J. T. SPARKS AND T. KOMOTO, *J. Appl. Phys.* **344**(2), 1191 (1962).
10. T. OHTANI, *J. Phys. Soc. Jpn.* **37**(3), 701 (1974).
11. R. BRUSETTI, J. M. D. COEY, G. CZJZEK, J. FINK, F. GOMPF, AND H. SCHMIDT, *J. Phys. F* **10**(1), 33 (1980).
12. P. TOULMIN AND P. B. BARTON, *Geochim. Cosmochim. Acta Suppl.* **28,** 641 (1964).
13. C. A. FRANCIS AND J. R. CRAIG, *Geol. Soc. Amer. Abst. Progr.* **8,** 176 (1976).
14. T. NODA, S. OHTOMO, K. IGAKI, AND W. T. HOLSER, *Tran. Jpn. Inst. Met.* **20**(3), 89 (1979).
15. G. COLLIN, G. CHAVANT, AND F. KELLER-BESREST, *Bull. Miner.* **103,** 380 (1980).
16. G. COLLIN, C. CHAVANT, AND R. COMES, *Acta Crystallogr. Sect. B* **39,** 289 (1983).
17. A. PUTNIS, *Amer. Miner.* **61,** 322 (1981).
18. M. NAKANO, M. TOKONAMI, AND N. MORIMOTO *Acta Crystallogr.* **835,** 722 (1979).
19. P. GOODMAN AND A. F. MOODIE, *Acta Crystallogr. Sect. A* **30,** 280 (1974).
20. K. ISHIZUKA AND S. IIJIMA "39th Annual Proceedings, Electron Microscopy Society of America Atlanta," p. 96, Claitors, Baton Rouge, La., (1981).
21. J. GJONNES AND A. F. MOODIE, *Acta Crystallogr.* **19,** 65 (1965).